Force Feedback Control of a Robotic Needle Insertion into Layered Soft Tissues

Tangwen Yang, Lifang Xiao, Panfei Chen, Haifeng Zhu
Institute of Information Science Beijing Jiaotong University
Beijing, China
twyang@bjtu.edu.cn

Xingang Zhao, Guoli Song
the State Key Laboratory of Robotics, Shenyang Institute of Automation, CAS
Shenyang, China
zhaoxingang@sia.cn

Jianda Han
College of Artificial Intelligence Nankai Univeristy
Tianjin, China
hanjianda@nankai.edu.cn

Weiliang Xu
Department of Mechnaical Engineering University of Auckland
Auckland, Newzealand
p.xu@auckland.ac.nz

***Abstract*—In this study, a feedback control law is proposed to steer a robotic needle using force information from a fiber optic sensor. This sensor is integrated into the lumen at the distal end of the needle to measure the needle insertion force. The force signals are analyzed via wavelet transform to identify the boundaries of layered soft tissues in real time. The boundaries information is then used in the robotic needle steering scheme to reduce as much as possible the insertion force, and mitigate the risk of tissue injury. Porcine belly tissue phantoms are herein used in the *ex vivo* tests of robotic needle insertion, and comparative study has been done with and without insertion force feedback. Experimental results show that the force feedback control approach proposed reduces effectively the insertion force.**

Keywords—robotic needle insertion, force feedback control, wavelet transform, boundaries identification, layered tissue

I. INTRODUCTION

Many clinical procedures, such as brachytherapy, anesthesia and biopsies, insert a needle to a specific target location inside human body to implant radioactive seeds, deliver drugs or collect tissue samples through the conduit of the needle lumen [1]. Hence, accurate targeting is a critical issue, but the needle insertion force deforms soft tissues, making accurate targeting difficult. For the needles with bevel tip, the asymmetric force on the needle tip deflects the needle shaft as well, and the targeting procedure is further complicated [2]. Training and practice are mandatorily required *in prior* for a physician to be capable of performing accurate needle insertion. But, manual needle insertion seriously relies on the physician's kinaesthetic feedback, and is prone to poor placement, and requires multiple insertions, which causes catastrophic outcomes, like healthy tissue trauma. For example, poor needle targeting during biopsies leads to healthy tissue removal. Moreover, inaccurate seed placement during radioactive ablation destroys healthy instead of malignant tissue. Robotic needle steering appears to be a promising means to effectively improve targeting accuracy [3]. Robotic mechanisms outside the patient drive the needle from its base and control the needle insertion and/or rotation velocities. It overcomes the limitation of manual insertion errors due to the physicians' fatigue, hand tremor. Furthermore, it enables them to be far away from X-ray exposure. Robotic needle insertion has aroused lots of research interest in recent years, and finds potential applications in prostate biopsy, breast tumor ablation, deep brain stimulation and minimal invasive surgeries, etc.

However, visual limitation, patient physiological movement, and tissue deformation contribute to targeting errors during a percutaneous insertion procedure. Substantial effort is hence needed to reduce the targeting error and to make robotic needle clinically viable. For instance, various imaging modalities, including ultrasound [4], CT or fluoroscopy [5] and MRI [6] are used to guide the needle tip in 2D plane or 3D volume, therefore, image feedback is frequently used for preoperative trajectory planning and intraoperative guidance. Meanwhile, the interaction between the needle tip and soft tissue is also a critical aspect to steer a robotic needle [7]. So, an accurate needle-tissue contact model is helpful to govern their interaction. Virtual spring model [8] and non-holonomic bicycle model [9] have been adopted to model the interactive dynamics. Okamura et al. [10] obtained a force model of needle insertion in terms of insertion force data obtained from bovine liver phantoms. This model is comprised of three components, namely, the stiffness force, the friction and the cutting force. The stiffness force occurs before the penetration of the liver capsule, and was defined by a second-order polynomial. The friction was defined by a Karnopp model, while the cutting force, which is necessary for the needle tip to rupture the tissue, was thus obtained by subtracting the friction force from the total force measured after a needle is penetrated to soft tissue. But, friction, tissue deformation and needle deflection, as well as tissue inhomogeneity and anisotropy, make it difficult to model needle-tissue interaction precisely. Therefore, a model-based control law itself cannot meet the demand of accurate needle placement. Position and force feedback are thus introduced to implement a closed-loop needle insertion control.

As mentioned previously, needle placement can be obtained from guidance images, where needle is visible and can be extracted by image processing. However, there is a trade-off between image quality and computation load. Meanwhile, the interactive force at the needle tip is especially important to mitigate targeting error, too. Moreover, excessive force may cause tissue trauma, and arouse the concern of insertion safety. Initially, the contact force is measured at the needle drive end [8,11], not from the needle tip, because it is very challenging to integrate a conventional force sensor into the space-constrained needle tip. Most recently, optical fibre technology is applied to the area of sensing, and grows

XXX-X-XXXX-XXXX-X/XX/$XX.00 ©20XX IEEE
978-1-5386-7544-1/18/$31.00 ©2018 IEEE

increasingly in medical fields, due to its big advantages over electrical sensors, such as miniaturization, higher accuracy and resolution, immunity from electromagnetic interference and biocompatibility [12]. A fibre optic force sensor was devised in our lab to measure the interactive force at the tip of a needle, and to identify the types of soft tissue [13,14]. Herein, the force information is now fed back into the control loop to reduce the interactive force at the needle tip, for purpose of insertion safety.

II. WAVELET ANALYSIS OF FORCE SIGNALS

A. Insertion force meausrement

A fiber optic sensor was devised in our lab to implement real-time measurement of the force at the needle tip during insertion [13,14]. This force occurs as the needle is inserted into soft tissue. It has the anatomic structure information on the path of needle insertion. This information can be used to control the robotic needle motion, to reduce the interactive force and thus mitigate soft tissue mobility and the risk of tissue trauma

B. Mallat wavelet transformat of force signals

The force signal measured during a needle insertion increases gradually as the needle enters into a layer of soft tissue and then abruptly decreases as the needle penetrates to the next layer of tissue. As mentioned previously, soft tissue is inhomogeneous and anisotropic. The force transients are not stationary in time and frequency domains. Wavelet transform method is thus used here to analyze the interactive force patterns and the types of soft tissues. Mallat introduced a multi-resolution signal representation by constructing a orthogonal wavelet basis [15]. The multi-resolution wavelet is computed with a pyramidal algorithm based on convolutions with quadrature mirror filters. Hence, multi-resolution is represented graphically as a set of nested subspace column $\{V_j\}_{j\in N}$, as shown in Fig.1.

Supposed that the original signal is V_0, it is decomposed into two subspaces in the frequency domain,: low frequency V_1 and high frequency W_1. The low frequency subspace V_1 can be decomposed again into two subspaces, low frequency V_2 and high frequency W_2. The sequence of decomposition can be written as follows

$$V_0 = V_1 \oplus W_1, V_1 = V_2 \oplus W_2, V_2 = V_3 \oplus W_3, \cdots, \quad V_{N-1} = V_N \oplus W_N \qquad (1)$$

Because $\{V_j\}_{j\in N}$ is a multi-resolution analysis in $L^2(R)$ space, in terms of the theorem of Riesz basis Existence, there exists a unique function, $\varphi(\tau) \in L^2(R)$. Through the function, there exists the formula (2) that must be a standard orthonormal basis in the V_j. The formula (2) is given by

$$\varphi_{j,k} = 2^{-j/2}\varphi\left(2^{-j}t - k\right), k \in N \qquad (2)$$

where $\varphi(t)$ is the scaling function.

Let $\varphi(t)$ generate a multi-resolution analysis, so $\phi \in V_0$ also belongs V_{-1}. By formula (2), we know that $\{\varphi_{-1,k} : k \in N\}$ is a Riesz basis that belonged V_{-1} .Therefore, there exists a unique l^2 sequence $\{h(k)\}$, and makes scaling function $\varphi(t)$ satisfies two-scale relations:

$$\phi(t) = \sqrt{2}\sum_{k=-\infty}^{\infty} h(k)\phi(2t-k) \qquad (3)$$

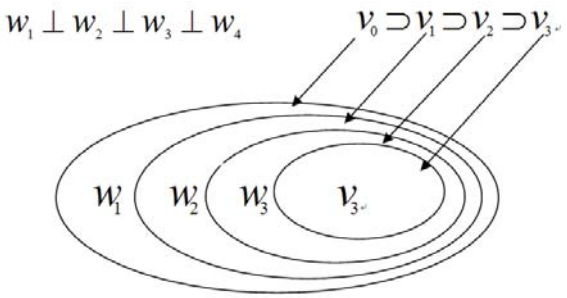

Fig. 1. nested multi-resolution subspace.

Since $V_{j+1} \in V_j, \forall j \in N$ ， $V_j = V_{j+1} \oplus W_{j+1}$, we can get the formula (4), given by

$$L^2(R) = \bigoplus_{j\in N} W_j \qquad (4)$$

Similarly, there exists a function $\psi(t)$ and let it generates the subspace W_0 ; Two-scale equation that belonged wavelet function $\psi(t)$ can be obtained:

$$\psi(t) = \sqrt{2}\sum_{k=-\infty}^{\infty} g(k)\phi(2t-k) \qquad (5)$$

The single $f(t) \in L^2(R)$， Suppose $A_j f \in V_j$ is a map of $f(t)$ based in 2^{-j} resolution, $\{V_j\}$ constitutes multi-resolution analysis of $L^2(R)$, so there exists the $V_j = V_{j+1} \oplus W_{j+1}$, that is

$$A_j f = A_{j+1} f + D_{j+1} f \,.$$

$$A_j f = \sum_{k=-\infty}^{\infty} C_{j,k}\psi_{j,k}(t), \quad D_j f = \sum_{k=-\infty}^{\infty} D_{j,k}\psi_{j,k}(t)$$

So, the formula (6) can be obtained:

$$\sum_{k=-\infty}^{\infty} C_{j,k}\varphi_{j,k}(t) = \sum_{k=-\infty}^{\infty} C_{j+1,k}\varphi_{j+1,k}(t) + \sum_{k=-\infty}^{\infty} D_{j+1,k}\psi_{j+1,k}(t) \qquad (6)$$

By formula (6), we can further have

$$\phi_{j+1,m}(t) = \sum_{k=-\infty}^{\infty} h(k-2m)\phi_{j,k}(t)$$

By scaling function orthogonality can be obtained:

$$\left\langle \phi_{j+1,m}, \phi_{j,k} \right\rangle = h(k-2m) \tag{7}$$

By formula (7) can be obtained:

$$\left\langle \psi_{j+1,m}, \phi_{j,k} \right\rangle = g(k-2m) \tag{8}$$

By formula (6-8) can be obtained:

$$C_{j+1,m} = \sum_{k=-\infty}^{\infty} C_{j,k} h^*(k-2m) \tag{9}$$

$$D_{j+1,m} = \sum_{k=-\infty}^{\infty} C_{j,k} g^*(k-2m) \tag{10}$$

$$C_{j,k} = \sum_{m=-\infty}^{\infty} h(k-2m) C_{j+1,m} + \sum_{m=-\infty}^{\infty} \sum_{m=-\infty}^{\infty} g(k-2m) D_{j+1,m} \tag{11}$$

The formula (9-11) can be expressed as：

$$\begin{cases} C_{j+1} = HC_j \\ D_{j+1} = GC_j \end{cases} \quad j = 0,1,\cdots,J \tag{12}$$

$$C_j = H^* C_{j+1} + G^* D_{j+1}, \qquad j = J, J-1, \cdots, 1, 0 \tag{13}$$

Formula (12) is a one-dimensional Mallat decomposition algorithm and formula (13) is a one-dimensional reconstruction algorithm.

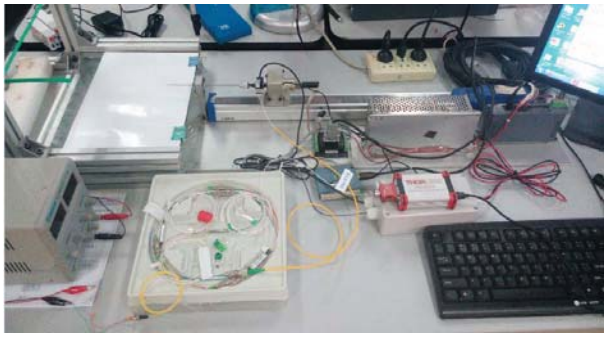

Fig. 2. Hardware components of the experimental setup.

III. Experiments and Result Analysis

A. Robotic needle insertion system

Experimental setup comprises a 2DOF needle insertion mechanism, a phantom tissue placement plate, the fiber optic force sensor and its optical link, PC computer, etc. as shown in Fig. 2. A graphical user interface for the robotic needle insertion system is implemented and shown in Fig.3. The insertion parameters such as the insertion distance, speed threshold can be set through the interface, and the force signal measured and its processing results with wavelet transform are illustrated as well.

Using the force signals and layer information, the robotic needle is steered. The force signals are first analyzed via a wavelet transform method to identify the boundaries of layered soft tissue. When the needle tip approaches the boundary of the layered tissue, the insertion force increases and alarm is turned on in terms of the specified risk level. The risk level is defined based on the interactive force information. If the insertion force is more than some threshold, the insertion will slow down or stop. As the force is reduced to a safe level, the insertion starts again. Therefore, the insertion force is all long under control, and reducing the risk of tissue injury.

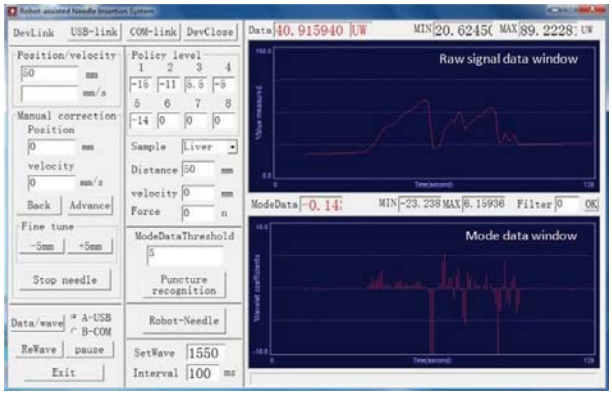

Fig. 3. The graphical user interface of the robotic needle insertion system.

B. Experimental data analysis

Porcine belly is typical layered tissue, as shown in Fig. 4, and used here as insertion phantom. There have six or seven layers, including the skin, the fat tissues and the muscles. Two types of experiments were conducted. In the 1st experiment, no force information is fed back into the robotic needle steering scheme. In the 2nd experiment, the feedback control approach makes use of the force information to restrict the insertion speed and force.

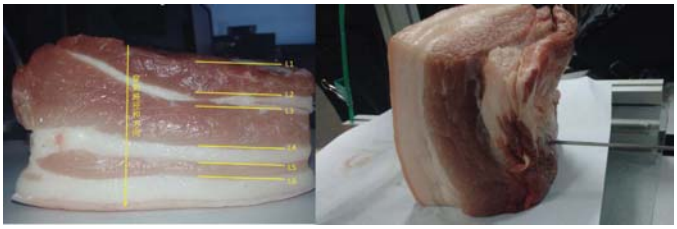

Fig. 4. Porcine belly tissue phantom.

a) Insertion experiment without force feedback

Before a needle insertion, the insertion parameters like distance, speed, etc. are required to specify through the user interface, and the force thresholds are set *a priori*, too. The tissue phantom is placed and nailed on the supporting plate. The acquired insertion force signals are illustrated on the user interface. Meanwhile, the signals are analyzed in real time through the Mallat wavelet transform algorithm. The boundaries of the layered tissue are identified in terms of the amplitudes of the wavelet coefficients, and are depicted on line.

Figure 5 shows the acquired insertion force as the needle is controlled to move at a constant speed, no force information used. It can be seen that, the insertion force is gradually increased as the needle tip is inserted into the tissue phantom,

causing the soft tissue to deform. Once the needle tip is completely entered into the tissue, there is a quick descent of the insertion force. When the deformation of the soft tissue is restored, the force is increasing again and the needle is entering into the second layer of the tissue phantom. When the insertion force decreases once again, it suggests that the needle has been inserted into the third layer, and so forth. The force transition generates a pattern mode, and corresponds well to the magnitude of the wavelet coefficient. It should be noted that the distance of two rising amplitudes reveals the thickness of a tissue layer.

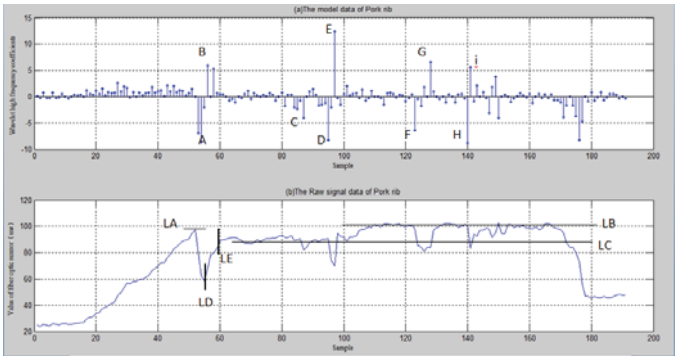

Fig. 5. The insertion force data and the boundaries of layered porcine belly tissue phantom, without force feedback.

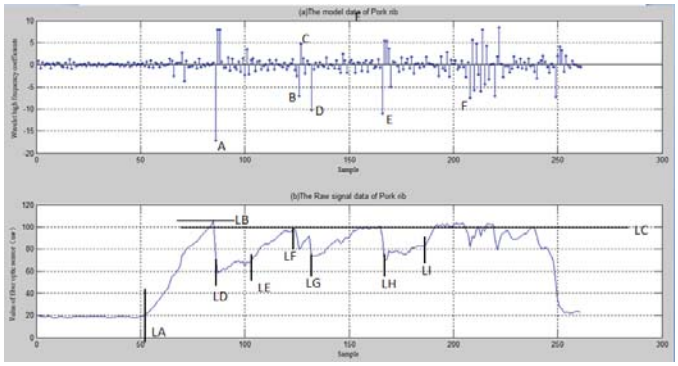

Fig. 6. The insertion force data and the boundaries of layered porcine belly tissue phantom, with force feedback.

b) Insertion experiment with force feedback

In this test, the boundaries information was used in the robotic needle steering to reduce as much as possible the insertion force and the risk of tissue injury. Fig.6 shows the experimental results of the controller with force feedback. As can be seen in Fig. 6(b), from LA to LB is the belly deformation process because of needle squeezing, from LB to LD, the force decreases instantly and generate mode data point A as shown in the Fig. 6(a). The point A triggers the control strategy, so the needle stops puncture immediately. From LD to LE can be seen that force is kept at a low level with waiting for soft tissue deformation recovery, so this policy can avoid the tissue damage caused by the movement of the needle when the tissue recovery and keep the force at a low level. LE is the end point of the policy and the needle began to move forward, so from LE to LF, the needle pierced in the muscle tip force begins to increase gradually. The point B show the needle pierced the layer L2.The point D show the needle pierced the layer L3 and trigger the policy, so the needle move forward at a low speed, from LG to LH, we can learn the force curve is relatively flat. The point E show the needle pierced the layer L4 and trigger the policy, so from LH to LI, the needle stop and the force curve keep at a low level.The value of the LC is maintained at a relatively stable level and less than the force threshold LB, so the feedback control of a robotically steered needle system can avoid the exceed force and reduce tissue damage.

IV. Conclusion

In this paper, a feedback control approach is proposed to steer a robotic needle using the information from a fiber optic force sensor. To accurately measure the insertion force, the sensor is integrated into the lumen at the distal end of the needle. Mallat wavelet transform is introduced here to analyze in real time the insertion force signals and to identify the boundaries of layered soft tissues. The boundaries information is then used in the robotic needle steering scheme. Porcine belly tissue phantoms were herein used in the ex-*vivo* tests of robotic needle insertion. Experimental results with and without insertion force feedback are presented, and show that the proposed feedback approach may effectively reduce the insertion force, thereby mitigating the risk of tissue injury.

Acknowledgment

This work is supported in part by the State's Key Project of Research and Development Plan (2017YFB130264-02), and the National Natural Science Foundation of China under grant 61375109.

References

[1] N. Abolhassani, R. Patel, and M. Moallem. "Needle insertion into soft tissue: A survey," Medical Engineering & Physics, 29, 1997, pp.413-431.

[2] T. Lehmann, C. Rossa, N. Usmani, et al., "Deflection modeling for a needle actuated by lateral force and axial rotation during insertion in soft phantom tissue," Mechatronics, 2017, 48:42-53.

[3] K. Cleary, V. Watson, D. Lindisch, et al., "Precision placement of instruments for minimally invasive procedures using a needle driver robot," Int. J. Medical Robotics and Computer Assisted Surgery, 2005, 1(2):40-47.

[4] G. Kichtinger, E. C. Burdette, et al., "Robotically assisted prostate brachytherapy with transrectal ultrasound guidance-Phantom experiments", Brachytherapy, 2006, 5:14-26.

[5] T. Hiraki, T. Matsuno, T. Kamegawa, et al., "Robotic insertion of various ablation needles under computed tomography guidance: accuracy in animal experiments", European Journal of Radiology, 2018, 105:162-167.

[6] H. Su, W. Shang, G. Li, "An MRI-guided telesurgery system using a Fabry-perot interferometry force sensor and a pneumatic haptic device", Annals of Biomedical Engineering, 2017, 45(8):1917-1928.

[7] S. P. DiMaio, S. E. Salcudean, "Interative simulation of needle insertion models", IEEE Transactions on Biomedical Engineering, 2005, 52(7): 1167-1179.

[8] Z. Neubach and M. Shoham, "Ultrasound guided robot for flexible needle steering", IEEE Transactions on Biomedical Engineering, 2010, 57(4): 799-805.

[9] R. J. Webster III, N. J. Cowan, G. Chirikjian, A. M. Okamura, “Non-holonomic modeling of needle steering”, Experimental Robotics IX, STAR 21, 2006, pp.35-44.

[10] A. Okamura, C. Simone, and M. O’Leary. “Force modeling for needle insertion into soft tissue,” IEEE Transactions on Biomedical Engineering, 2004, 51(10):1707-1716.

[11] D. Glozman and M. Shoham, “Image-guided robotic flexible needle steering”, IEEE Transactions on Robtics, 2007, 23(3): 459-467.

[12] P. Puangmali, K. Althoefer, L. D. Seneviratne, et al. “State-of-the-art in force and tactile sensing for minmally invasive surgery,” IEEE Sensor Jounal, 8(4), 2008, pp. 371-381.

[13] T. W. Yang, H. F. Zhu, J. D. Han, et al. “Identification of tissue types and boundaries with a fiber optic force sensor,” Science China - Information Sciences, 57(12), 2014, pp.120206(7).

[14] T. W. Yang, P. F. Chen, J. D. Han and W. L. Xu, “Wavelet transform analysis of optic fiber force sensing signals at pucture needle tip,” Optics and Precision Engineering, 23(8), 2015, pp.2149-2157.

[15] S. Mallat, “A wavelet tour of signal processing,” Academica Press, San Diego CA, 1998.